Majorana fermion realization and relevant transport processes in a triple-quantum dot system*

Deng Ming-Xun(邓明勋), Zheng Shi-Han(郑诗菡), Yang Mou(杨 谋),
Hu Liang-Bin(胡梁宾), and Wang Rui-Qiang(王瑞强)†

Laboratory of Quantum Engineering and Quantum Materials, ICMP and SPTE, South China Normal University, Guangzhou 510006, *China*

(Received 18 August 2014; revised manuscript received 10 October 2014; published online 9 January 2015)

Nonequilibrium electronic transports through a system hosting three quantum dots hybridized with superconductors are investigated. By tuning the relative positions of the dot levels, we illustrate the existence of Majorana fermions and show that the Majorana feimions will either survive separately on single dots or distribute themselves among different dots with tunable probabilities. As a result, different physical mechanisms appear, including local Andreev reflection (LAR), cross Andreev reflection (CAR), and cross resonant tunneling (CRT). The resulting characteristics may be used to reveal the unique properties of Majorana fermions. In addition, we discuss the spin-polarized transports and find a pure spin current and a spin filter effect due to the joint effect of CRT and CAR, which is important for designing spintronic devices.

Keywords: Majorana fermion, quantum dots hybridized with superconductors, spin-polarized transports

PACS: 73.21.La, 74.45.+c, 73.23.Hk **DOI:** 10.1088/1674-1056/24/3/037302

1. Introduction

Majorana fermions (MFs), with criteria of self-Hermitian and zero-energy, are predicted to be realized in condensed matter systems by combining strong spin–orbit interaction, broken time-reversal symmetry, and superconductivity.[1–6] With their nonlocality, a pair of spatially well-separated MFs can encode a qubit, which has a great potential in fault-tolerant topological quantum computation, since the qubit encoded by MFs is robust against decoherence due to local perturbations.[7] As a consequence, searching for and controlling of the new type of particles with non-Abelian statistics are recently receiving much attention.[2–11]

Since quasiparticles in superconductors are the superposition of electron and hole components with invariance for the exchange of the electron and hole components, superconductors provide a powerful platform to realize MFs.[12] Recently, it was predicted that Majorana bound states (MBSs) can survive at both ends of a one-dimensional (1D) semiconducting wire or the edges of a two-dimensional (2D) quantum spin Hall insulator by combining the spin–orbit coupling and the proximity effect induced by the conventional s-wave superconductor,[4,6,13] and the features of the topological ends or edges can be detected via electronic transport.[14–16] By decoupling the Kitaev model[17] to a series of quantum dots (QDs) with the gate-tunable level connected by s-wave superconductors, MFs that are protected by a disorder robust topological gap can be realized at the ends of the quantum dot chain.[18,19] For the simplest case, the system with two QDs connected by an s-wave superconductor has been investigated. It is shown that the poor man's MBSs can form on the dots under appropriate conditions, and they share all the characteristics of the standard MBSs, only lacking the topological protection.[20]

The nonlocality of MFs is usually hard to probe by electrical measurement.[21–24] However, when they are well separated, superpositions of MF pairs can form a nonlocal fermion level. As a result, the cross correlation is introduced to certify the nonlocality of MFs. It is addressed that the nonlocality of a pair of MBSs can be probed in conductance as well as noise cross correlation for cross Andreev reflection (CAR).[25,26] Among these, the use of quantum dots to probe MFs is widely studied.[10,18,19,25–34] For instance, two QDs are inserted between a nanowire's ends hosting MFs and metal leads to suppress the effect from the local Andreev reflection (LAR).[27,28] For the case of weak dot–reservoir coupling, it is found that the cross correlation can be both negative and positive, depending on the quantum dots' relative levels.[27] For strong dot–reservoir coupling, the cross correlation exhibits a clover-like shape,[28] and vanishes when one of the dot levels is in resonance with the Majorana zero mode.[26]

In this paper, we study a system consisting of three QDs connected to two conventional superconductors. By tuning the relative position of the dot levels, we demonstrate the existence of MFs and show that the MFs either survive on a single dot separately or extend themselves among different dots with tunable probabilities. As a result, there are different physical mechanisms, including the LAR, CAR, and cross resonant

*Project supported by the New Century Excellent Talents in University of China (Grant No. NCET-10-0090), the National Natural Science Foundation of China (Grant Nos. 11474106, 11174088, and 11274124), the Program for Changjiang Scholars and Innovative Research Team in University of China (Grant No. IRT1243), and the Natural Science Foundation of Guangdong Province, China (Grant No. S2012010010681).

†Corresponding author. E-mail: wangrqgz@163.com

© 2015 Chinese Physical Society and IOP Publishing Ltd

tunneling (CRT). These mechanisms are modulated by MBSs and can be switched to each other by tuning the system parameters, which characterizes the unique properties of MFs. In addition, spin-polarized transports are discussed, and a pure spin current and the spin filter effect are presented as a result of the combination of CRT and CAR.

The paper is organized as follows: in Section 2, we establish a theoretical model and search for the realization of MBSs. The different mechanism governed average currents, shot noise, and spin-dependent transports are discussed in Section 3. In the last section, a short summary is given.

2. Model and methods

We consider a system of three coupling QDs connected to two conventional superconductors, as schematically shown in Fig. 1. The coherent lengths of the superconductors are assumed to be larger than their geometric lengths so as to allow the CAR related to electrons on different dots. The superconductors are grounded, and the two ends of the system (dot 1 and dot 2) are respectively connected to, via tunnel coupling, two normal metal leads with chemical potential $\mu_{\mathrm{L(R)}}$ (not shown in Fig. 1).

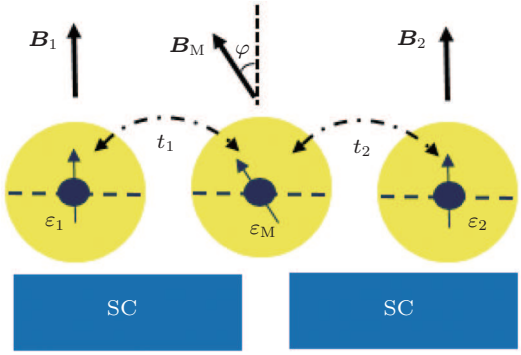


Fig. 1. (color online) Sketch of setup. Three tunnel-coupling quantum dots are connected to two grounded conventional superconductors. Both ends of the system (dot 1 and dot 2) are tunnel-coupled to two normal metal leads (not shown) with chemical potential $\mu_{\mathrm{L(R)}}$. To search for MFs, each dot is fully spin-polarized by an applied magnetic field. The magnetic fields on the outer dots are parallel with each other and have an angle φ with respect to that on the middle dot.

The Hamiltonian of the system under investigation is written as $H = H_{\mathrm{lead}} + H_{\mathrm{cent}} + H_{\mathrm{lead-cent}}$, including the Hamiltonian of the normal metal reservoirs with dispersion spectrum $\varepsilon_{\alpha,k}$ ($H_{\mathrm{lead}} = \sum_{\alpha\in\mathrm{L,R}}\sum_{k\sigma}\varepsilon_{\alpha,k}c^{\dagger}_{\alpha,k\sigma}c_{\alpha,k\sigma}$), the Hamiltonian of the central region (H_{cent}), and that of coupling between them with coupling strength V_α ($H_{\mathrm{lead-cent}} = \sum_{k\sigma}V_{\mathrm{L}}c^{\dagger}_{\mathrm{L},k\sigma}d_{1\sigma} + V_{\mathrm{R}}c^{\dagger}_{\mathrm{R},k\sigma}d_{2\sigma} + \mathrm{H.c}$). In the central region, all quantum dots are assumed to be single-occupied at level $\varepsilon_{i\sigma}$ due to the strong Coulomb interaction. To search for Majorana fermions in such a system, each dot is spin-polarized by an applied magnetic field $\boldsymbol{B}_i$, with $\boldsymbol{B}_1$ parallel to $\boldsymbol{B}_2$ but deviating from $\boldsymbol{B}_{\mathrm{M}}$ with an angle φ (see Fig. 1). This specific arrangement can modify both the CAR and the single-particle tunneling, so the Hamiltonian H_{cent} of the central region reads[35]

$$\begin{aligned} H_{\mathrm{cent}} = & \sum_{i=1,2,\mathrm{M};\sigma}\varepsilon_{i\sigma}d^{\dagger}_{i\sigma}d_{i\sigma} \\ & + \sum_{i=1,2;\sigma} t_i d^{\dagger}_{i\sigma}[\cos(\varphi/2)d_{\mathrm{M}\sigma} \\ & + \sigma_z \sin(\varphi/2)d^{\dagger}_{\mathrm{M}\bar{\sigma}}] \\ & + \Delta_i d_{i\sigma}[\bar{\sigma}_z \sin(\varphi/2)d_{\mathrm{M}\sigma} \\ & + \cos(\varphi/2)d^{\dagger}_{\mathrm{M}\bar{\sigma}}] + \mathrm{H.c.}, \end{aligned} \tag{1}$$

where $\sigma_z, \bar{\sigma}_z = \pm$, the pairing potential $\Delta_{1(2)}$ between the dots are induced by the proximity effect of the superconductors, and the tunneling amplitudes $t_{1(2)}$ are the values for parallel fields. Here, the single-particle tunneling between dots and superconductors is neglected as we limit the transport within the superconductor gap.

Firstly, we assume the Zeeman splitting to be larger than the temperature, for which only one spin level, e.g., $\sigma = \downarrow$, is within the window of transport. In this case, Hamiltonian (1) is reduced to a spinless model as in Ref. [20]

$$\begin{aligned} H_{\mathrm{cent}} = & \sum_{i=1,2,\mathrm{M}}\varepsilon_i d^{\dagger}_i d_i \\ & + \sum_{i=1,2}(t_i d^{\dagger}_{i\sigma}d_{\mathrm{M}\sigma} + \Delta_i d_{i\sigma}d_{\mathrm{M}\sigma} + \mathrm{H.c.}), \end{aligned} \tag{2}$$

where for simplicity the dependence on φ has been absorbed into t_i and Δ_i, which is reflected by the tunable ratio Δ_i/t_i.

In a Nambu presentation, Hamiltonian (2) can be expressed as

$$H_{\mathrm{cent}} = \frac{1}{2}(\Psi \boldsymbol{h} \Psi^{\dagger} + \varepsilon_1 + \varepsilon_{\mathrm{M}} + \varepsilon_2) \tag{3}$$

under the basis $\Psi = (d^{\dagger}_1, d^{\dagger}_{\mathrm{M}}, d^{\dagger}_2, d_1, d_{\mathrm{M}}, d_2)$ with

$$\boldsymbol{h} = \begin{pmatrix} \varepsilon_1 & t_1 & 0 & 0 & \Delta_1 & 0 \\ t_1 & \varepsilon_{\mathrm{M}} & t_2 & -\Delta_1 & 0 & \Delta_2 \\ 0 & t_2 & \varepsilon_2 & 0 & -\Delta_2 & 0 \\ 0 & -\Delta_1 & 0 & -\varepsilon_1 & -t_1 & 0 \\ \Delta_1 & 0 & -\Delta_2 & -t_1 & -\varepsilon_{\mathrm{M}} & -t_2 \\ 0 & \Delta_2 & 0 & 0 & -t_2 & -\varepsilon_2 \end{pmatrix}, \tag{4}$$

where we have assumed the superconductors have the same phase and so choose Δ_i and t_i to be real for simplicity. We diagonalize the Hamiltonian $\boldsymbol{h}$ and solve the corresponding Bogoliubov–de Gennes equation[18,26]

$$\boldsymbol{h}\boldsymbol{\Phi} = \lambda\boldsymbol{\Phi} \tag{5}$$

with $\boldsymbol{\Phi} = (\Phi_1, \Phi_2, \Phi_3, \Phi_4, \Phi_5, \Phi_6)$ to search for zero-energy quasiparticles of Majorana states. Then the quasiparticle operators can be expressed as $\gamma_i = \boldsymbol{\Phi}_i \cdot \boldsymbol{\Psi}^{\dagger}$.

When the levels of dot 1 and dot 2 are aligned with the chemical potential of the superconductors ($\mu_{\mathrm{S}} = 0$), namely, $\varepsilon_1 = \varepsilon_2 = 0$, we can always find two zero-energy solutions to Eq. (5) for $t_i = \Delta_i$, reading

$$\gamma_1 = (d^{\dagger}_1 + d_1)/\sqrt{2}, \quad \gamma_2 = \mathrm{i}(d^{\dagger}_2 - d_2)/\sqrt{2}. \tag{6}$$

They clearly obey the Majorana criterion $\gamma^{\dagger}_{1(2)} = \gamma_{1(2)}$, and therefore describe MBSs. Interestingly, one can notice that the two Majorana states are well spatially separated since γ_1 and γ_2 are completely localized on dot 1 and dot 2, respectively. Furthermore, these states are independent of the middle dot level ε_M. If we loosen the constraint and only set $\varepsilon_2 = 0$, there are still two zero-energy states, which can be reduced to

$$\begin{aligned}\gamma_1 &= -\frac{\delta\beta}{\sqrt{2}}(d_1^{\dagger}+d_1)+\frac{\beta}{\sqrt{2}}(d_M^{\dagger}+d_M),\\ \gamma_2 &= \mathrm{i}(d_2^{\dagger}-d_2)/\sqrt{2}\end{aligned} \tag{7}$$

for $\varepsilon_M = 0$, where we denote $\delta = 2\Delta_1/\varepsilon_1$ and $\beta = 1/\sqrt{(1+\delta^2)}$. Obviously, γ_1 and γ_2 are still Majorana states. Interestingly, in spite of γ_2 completely remaining on dot 2, γ_1 is no more only located on dot 1, some weight ($\sim \beta/\sqrt{2}$) is transferred to the middle dot. This implies that we can distribute the Majorana states among different dots with tunable weight determined by the dot levels.

To compute the transport properties, we switch to the many-particle presentation on the basis $|n_1 n_M n_2\rangle$, where $n_{1,M,2} = 0$ or 1 represents the occupation of the QDs. Without lead–dot couplings, the parity of the central region is conserved though the particles are not invariant, since the electrons are absorbed into or split out from the superconductors in pairs. Therefore, the Hamiltonian of the central region $H_{\rm cent}$ is block diagonal in the Hilbert space spanned by the parity subspace, namely,

$$\boldsymbol{H}_{\rm cent} = \begin{pmatrix} \boldsymbol{H}_{\rm e} & 0 \\ 0 & \boldsymbol{H}_{\rm o} \end{pmatrix}. \tag{8}$$

Here $\boldsymbol{H}_{\rm e}$ for even parity subspace

$$|\Omega\rangle^{\rm e} = \{|000\rangle, |011\rangle, |110\rangle, |101\rangle\}$$

and $\boldsymbol{H}_{\rm o}$ for odd parity subspace

$$|\Omega\rangle^{\rm o} = \{|010\rangle, |001\rangle, |100\rangle, |111\rangle\}$$

are given by

$$\boldsymbol{H}_{\rm e} = \begin{pmatrix} 0 & \Delta_2 & \Delta_1 & 0 \\ \Delta_2 & \varepsilon_2+\varepsilon_M & 0 & t_1 \\ \Delta_1 & 0 & \varepsilon_1+\varepsilon_M & t_2 \\ 0 & t_1 & t_2 & \varepsilon_1+\varepsilon_2 \end{pmatrix}, \tag{9}$$

$$\boldsymbol{H}_{\rm o} = \begin{pmatrix} \varepsilon_M & t_2 & t_1 & 0 \\ t_2 & \varepsilon_2 & 0 & \Delta_1 \\ t_1 & 0 & \varepsilon_1 & \Delta_2 \\ 0 & \Delta_1 & \Delta_2 & \varepsilon_1+\varepsilon_2+\varepsilon_M \end{pmatrix}. \tag{10}$$

The diagonalized master equation approach extending the infinite-bias limit to an arbitrary bias voltage[27,29,30,36,37] is adopted. Firstly, by diagonalizing the Hamiltonian $\boldsymbol{H}_{\rm e}$ ($\boldsymbol{H}_{\rm o}$), we obtain the eigenvectors $|e_i\rangle$ ($|o_j\rangle$), i.e.,

$$\begin{aligned}|e_i\rangle &= e_{i1}|000\rangle + e_{i2}|011\rangle + e_{i3}|110\rangle + e_{i4}|101\rangle,\\ |o_j\rangle &= o_{j1}|010\rangle + o_{j2}|001\rangle + o_{j3}|100\rangle + o_{j4}|111\rangle.\end{aligned} \tag{11}$$

The lead–dot Hamiltonian $H_{\rm lead-cent}$ mixes the states of different blocks via breaking the parity conservation and contributes to the current by tunneling the matrix elements

$$\begin{aligned}\langle e_i|d_1|o_j\rangle &= e^*_{i1}o_{j3} + e^*_{i2}o_{j4},\\ \langle e_i|d_2|o_j\rangle &= e^*_{i1}o_{j2} + e^*_{i3}o_{j4},\\ \langle o_j|d_1|e_i\rangle &= o^*_{j1}e_{i3} + o^*_{j2}e_{i4},\\ \langle o_j|d_2|e_i\rangle &= o^*_{j1}e_{i2} + o^*_{j3}e_{i4},\end{aligned} \tag{12}$$

with $\langle e_i|d_i|e_j\rangle = 0$ and $\langle o_i|d_i|o_j\rangle = 0$. We consider the case of weak lead–dot coupling, $\Gamma_\alpha \le k_{\rm B}T_\alpha, t_i$, so that the current and the shot noise properties of the system are determined by the reduced density matrix $\rho_{\rm cent}$, $\rho_{\rm cent} = \sum_l P_l|l\rangle\langle l|$ ($|l\rangle \in \{|e_i\rangle\}, |o_j\rangle\}$) with P_l the probability of finding the central state at $|l\rangle$. Then, we gather all the probabilities as a column vector $\boldsymbol{P}$, thus, the matrix form of the rate equations can be written as

$$\frac{{\rm d}\boldsymbol{P}(t)}{{\rm d}t} = \boldsymbol{W}\cdot\boldsymbol{P}(t), \tag{13}$$

with the matrix elements

$$\begin{aligned}W_{ll'} = &\sum_{\alpha={\rm L,R}}\sum_{i=1,2}\delta_{\alpha,i}\Gamma_\alpha[f(\varepsilon_l-\varepsilon_{l'}-\mu_\alpha)|\langle l'|d_i|l\rangle|^2\\ &+(1-f(\varepsilon_{l'}-\varepsilon_l-\mu_\alpha))|\langle l|d_i|l'\rangle|^2],\end{aligned} \tag{14}$$

and $W_{ll} = -\sum_{l'\neq l}W_{l'l}$. Here, $\delta_{\alpha,i} = 1$ for $\alpha = $ L (or R) and $i = 1$ (or 2), and $\delta_{\alpha,i} = 0$ otherwise, $\varepsilon_i^{(\rm e)}$ ($\varepsilon_j^{(\rm o)}$) is the eigenvalue corresponding to eigenvector $|e_i\rangle$ ($|o_j\rangle$), $f(x) = (\mathrm{e}^{\frac{x}{k_{\rm B}T}}+1)^{-1}$, and $\Gamma_\alpha = 2\pi D_\alpha|V_\alpha|^2$ with D_α being the density of the states of electron in the α lead. When the system reaches the dynamic equilibrium, $\dot{\boldsymbol{P}}(t) = 0$, we can solve out $\boldsymbol{P}$ under the normalization condition $\sum_i P_i = 1$. Finally, the current through the α lead is calculated by

$$I_\alpha = \sum_k[\hat{\boldsymbol{I}}_\alpha\cdot\boldsymbol{P}]_k, \tag{15}$$

where the summation goes over all vector elements k. The $\hat{\boldsymbol{I}}_\alpha$ is the matrix form of the current operator, whose matrix elements have similar expressions as $W_{ll'}$ in Eq. (14), only replacing the positive sign $+$ with negative sign $-$ and taking $\alpha = $ L or R.

With the combination-generation approach,[38–40] the noise correlators are given by

$$\begin{aligned}S_{I_\alpha I_{\alpha'}}(\omega) = &\ 2\delta_{\alpha\alpha'}|\sum_k[\hat{\boldsymbol{I}}_\alpha\cdot\boldsymbol{P}]_k| + 2\sum_k[\hat{\boldsymbol{I}}_{\alpha'}\hat{\boldsymbol{T}}(-\omega)\hat{\boldsymbol{I}}_\alpha\cdot\boldsymbol{P}\\ &+\hat{\boldsymbol{I}}_\alpha\hat{\boldsymbol{T}}(\omega)\hat{\boldsymbol{I}}_{\alpha'}\cdot\boldsymbol{P}]_k\end{aligned} \tag{16}$$

with $\hat{\boldsymbol{T}}(\pm\omega) = 1/(\mp{\rm i}\omega\boldsymbol{I}-\boldsymbol{W})$, where the first term is the frequency-independent Schottky noise originated from the self-correlation of a given tunneling event, and $\boldsymbol{I}$ is the unit matrix.

3. Numerical results and discussion

With numerical calculations, we discuss the case of symmetrical tunnel coupling $\Gamma_L = \Gamma_R = \Gamma_0 \leq k_B T_0$ (in experiments, the lead–dot coupling energy is $\Gamma_0 \sim 0.01$ meV[41,42]), where $T_L = T_R = T_0$, and we set $\Delta_1 = \Delta_2 = \Delta_0$ and $t_1 = t_2 = t_0$ for the sake of simplicity.

3.1. MBS-modulated transport

The calculated current I_α through the α lead and the net current $I_{\rm net} = I_L + I_R$ through the superconductors are plotted as a function of dot levels ε_1 and ε_2 in Fig. 2. Figures 2(a) and 2(b) indicate that $I_{L(R)}$ exhibits maximal absolute values around $\varepsilon_{1(2)} = 0$. It is attributed to the LAR process with a pair of electrons absorbed by or emitted from the same lead. For the original point $\varepsilon_1 = \varepsilon_2 = 0$, from Eq. (6), we know that two uncoupled MBSs are located respectively on dot 1 and dot 2, and so I_L and I_R reach the maximal values regardless of ε_M. In the limit of $\mu_L = -\mu_R \to \infty$, the current solution can be analytically expressed as $|I_{L(R)}| = \Gamma_{L(R)}/2$. LAR's local feature is also manifested by zero-frequency cross current correlation $S_{LR}(0) = 0$ (see Fig. 2(f)). When we keep $\varepsilon_M = 0$ and let either dot level align with the superconductor one, e.g., $\varepsilon_2 = 0$, as shown in Fig. 3(a), the variation of ε_1 away from zero does not influence I_R, but reduces I_L from a peak to zero quickly. This can be understood based on Eq. (7), i.e., tuning of ε_1 transfers the weight of the Majorana wave function γ_1 from dot 1 to the middle dot, but is irrelevant to MBS γ_2 on dot 2. For finite ε_M and $\varepsilon_2 = 0$, I_R exhibits a similar scenario of current peak as in I_L out of the same reason, namely, the weight of γ_2 distributes between dot 2 and dot M at $\varepsilon_M \neq 0$. For the general case of finite ε_M and ε_2, as depicted in Figs. 3(b)–3(d), the LAR current peak is sensitive to ε_M and vanishes for $\varepsilon_M > 0.25$ meV.

In Figs. 2(a) and 2(b), apart from the LAR current peaks along the axis, one can simultaneously notice that there emerge two types of subpeaks: a negative one (electron tunnels out of the central region to the leads) along the diagonal region ($\varepsilon_1 = \varepsilon_2$) and a positive value (electron tunnels into the central region from the leads) along the anti-diagonal region ($\varepsilon_1 = -\varepsilon_2$). What is more, for the former, I_L has the same value as I_R but with an opposite sign, obeying $I_L = -I_R$, thus $I_{\rm net} = 0$ holds exactly. While for the latter case, $I_L = I_R$ holds strictly. These relations can also be seen in Figs. 3(b)–3(d). In fact, different physical mechanisms exist. Physically, $I_L = I_R$ implies a CAR process, while $I_L = -I_R$ is for electron tunneling from the left lead to the right lead. To distinguish them, we further plot the dependence of I_L on ε_1 and ε_2 for $t_0 = 0$ (Fig. 2(d)) and $\Delta_0 = 0$ (Fig. 2(e)), where the anti-diagonal peak vanishes and only the diagonal peak remains. For $t_0 = 0$, an electron tunnels from dot 1 to dot 2 through absorbing and splitting Cooper pairs simultaneously, while for $\Delta_0 = 0$, an electron tunnels via the middle dot normally. These two cases cannot form the CAR process but with a resonant tunneling feature, so we name them as cross resonant tunneling (CRT). For the former, the arrangement of $\varepsilon_1 = \varepsilon_2 = -\varepsilon_M$ is in favor of the formation of zero-energy Cooper pairs between dot 1 (or dot 2) and the middle dot, thus there appears a current resonance region around $\varepsilon_1 = \varepsilon_2 = -\varepsilon_M$, see Fig. 2(d). For the latter, the identical level of $\varepsilon_1 = \varepsilon_2 = \varepsilon_M$ favors the resonant tunneling through the middle dot, so exhibiting a current resonance here, see Fig. 2(e). In contrast, for the arrangement of $\varepsilon_1 = -\varepsilon_2$, a pair of electrons from two dots have zero total energy and so can form a Cooper pair entering into the superconductor together. As a result, I_L and I_R have the same value and sign.

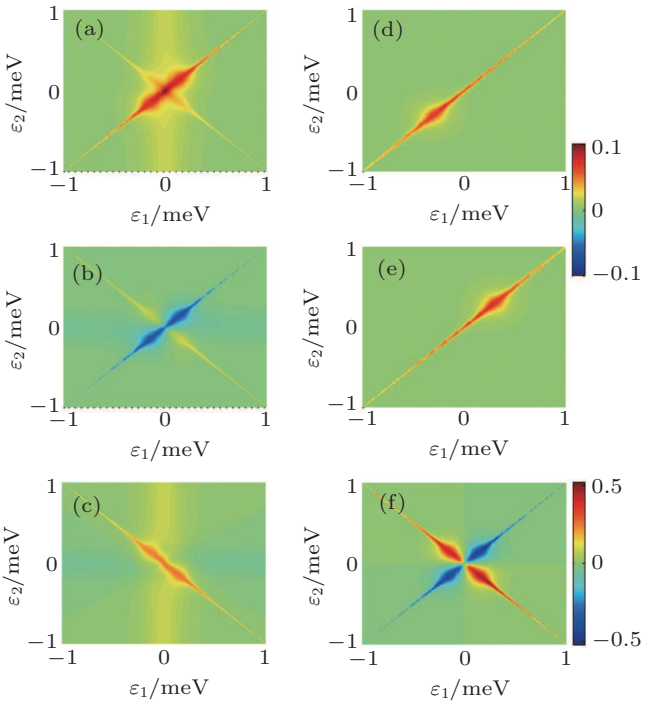


Fig. 2. (color online) Currents (a) I_L, (b) I_R, and (c) $I_{\rm net}$ as a function of dot levels ε_1 and ε_2 for $t_0 = \Delta_0 = 0.05$ meV, and I_L for (d) $t_0 = 0$ and (e) $\Delta_0 = 0$. (f) Zero-frequency cross current correlations $S_{LR}(0)$. Other parameters are $\Gamma_0 = 0.01$ meV, $\varepsilon_M = 0.15$ meV, $\mu_L = 0.2$ mV, $\mu_R = -0.1$ mV, and $k_B T_0 = 0.5$ meV ($T_0 \sim 5.8$ K) expected for the specific indication.

In Fig. 2(f), the zero-frequency current noise cross correlation $S_{LR}(0)$ is displayed in the ε_1–ε_2 plane. Interestingly, different physical processes are characterized. The CAR process involved in the electron pair movement is a positive correlation, while the CRT tends to tunnel into one dot and out of the other. The opposite tunnelings generate negative correlations. Therefore, in a whole, $S_{LR}(0)$ exhibits a quadrupole pattern with alternating positive and negative values. This pattern is robust against the bias setting applied to the normal leads.

Interestingly, the bias setting has a great influence on the currents. In Fig. 3(c), we illustrate the variation of the currents for different chemical potentials of the right lead (μ_R) by fixing μ_L at 0.2 mV. By tuning μ_R, the weight of the current

peaks of CAR and CRT, respectively located at $\varepsilon_1 = -\varepsilon_2$ and $\varepsilon_1 = \varepsilon_2$, can be redistributed between them. For $\mu_R = -\mu_L$, the CAR current peak is completely suppressed (see the short-dot lines in Fig. 3(c)) due to the opposite movement of electrons in different leads. As we increase μ_R from $\mu_R = -\mu_L$, the CAR current peak increases gradually, while the CRT current peak is reduced correspondingly (see the solid lines in Fig. 3(c)) and eventually vanishes at $\mu_R = \mu_L$, which favorably provides the electrons with the same direction and so favors the CAR process (see the dash-dot lines in Fig. 3(c)). Therefore, mediating μ_R can be applied to observe the transition between the CRT and CAR mechanisms. In addition, we plot the dependences of the currents on ε_M and t_0 respectively in Figs. 3(b) and 3(d), where the increase in ε_M and t_0 is only to widen the resonant peaks, irrelevant to the peak height. Our numerical calculations also show that with the increase in temperature, the LAR current peaks will decrease, while the CAR and CRT current peaks will increase to maximum values before reducing.

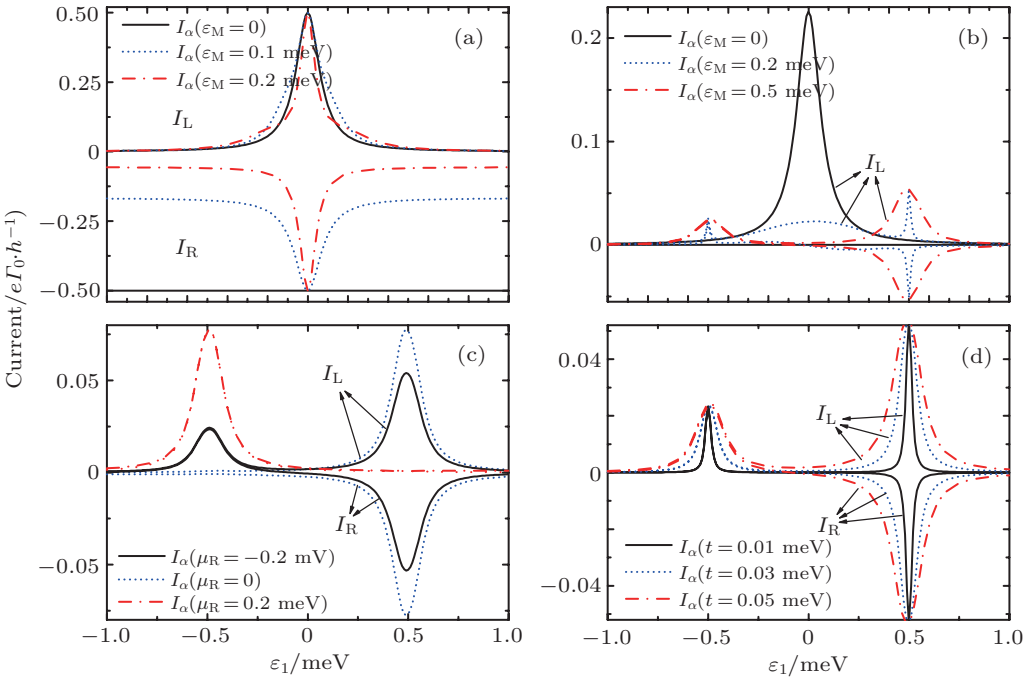


Fig. 3. (color online) Currents I_L and I_R as a function of ε_1 for different ε_M with (a) $\varepsilon_2 = 0$ (I_L: positive, I_R: negative) and (b) $\varepsilon_2 = 0.5$ meV; for (c) different μ_R and (d) different t ($t_0 = \Delta_0 = t$) with $\varepsilon_M = 0.5$ meV. The other parameters are $t_0 = \Delta_0 = 0.05$ meV, $\mu_L = 0.2$ mV, $\mu_R = 0, k_B T_0 = 0.2$ mV ($T_0 \sim 2.3$ K), and $\Gamma_0 = 0.01$ meV expected for the specific indication.

3.2. Triple-QD modulated spin-resolved transports

From the above analysis, we know that there are two different physical mechanisms contributing to the current in the right lead with opposite flowing directions. This makes one recall the generation of a pure spin current where two spin species transfer with the same magnitude but opposite directions. In order to generate a pure spin current, we set the spin-degenerated dot levels $\varepsilon_{1\sigma} = \varepsilon_1$ and $\varepsilon_{M\sigma} = \varepsilon_M$, while the spin levels $\varepsilon_{2\uparrow(\downarrow)} = \varepsilon_2 \mp \Delta_B/2$ on the right dot are lifted by Zeeman energy Δ_B which is tuned to be comparable with other parameters. Consequently, both spin species take part in the transport, as depicted schematically in Fig. 4. For the right lead, if setting $\varepsilon_2 = 0$ and ε_1 align with $\varepsilon_{2\downarrow}$, spin-down electrons tunnel from the left lead to the right lead via the CRT mechanism, contributing the forward spin-down current. At the same time, $\varepsilon_1 = -\varepsilon_{2\uparrow}$ is also satisfied and so the CAR mechanism generates the backward spin-up current. Thus a pure spin current emerges in the right lead when $I_{R\uparrow} = -I_{R\downarrow}$.

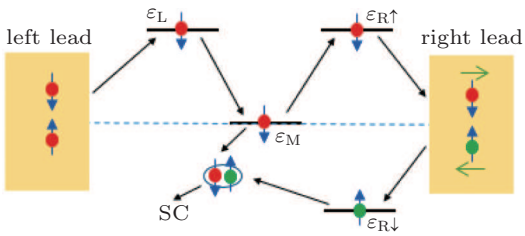


Fig. 4. (color online) Schematic diagram of generation of a pure spin current when both spin levels contribute to the transport.

The above arguments are confirmed by the following numerical results. We start with the full spin Hamiltonian in Eq. (1), whose block diagonal matrices in Eq. (8), under the basis $|n_1^\sigma n_2^\sigma n_M^\sigma\rangle$ with $n_{1,2,M}^\sigma = 0, \uparrow, \downarrow$, are 13×13 $\boldsymbol{H}_e$ and 14×14 $\boldsymbol{H}_o$. We still employ the rate equation (13) to obtain the occupied probability for eigenstate $|l\rangle$ of $\boldsymbol{H}_{cent}$ with

the transition matrix elements

$$W_{ll'} = \sum_{\alpha=\mathrm{L,R}} \sum_{i=1,2;\sigma} \delta_{\alpha,i}\Gamma_\alpha [f(\varepsilon_l - \varepsilon_{l'} - \mu_\alpha)|\langle l'|d_{i\sigma}|l\rangle|^2 + (1 - f(\varepsilon_{l'} - \varepsilon_l - \mu_\alpha))|\langle l|d_{i\sigma}|l'\rangle|^2]. \quad (17)$$

The spin-dependent current $I_{\alpha\uparrow(\downarrow)}$ is calculated by

$$I_{\alpha\sigma} = \sum_k [\hat{\boldsymbol{I}}_{\alpha\sigma} \cdot \boldsymbol{P}]_k, \quad (18)$$

where the current matrix $\hat{\boldsymbol{I}}_{\alpha\sigma}$ is spin dependent with matrix elements

$$(\hat{\boldsymbol{I}}_{\alpha\sigma})_{ll'} = \sum_{i=1,2} \delta_{\alpha,i}\Gamma_\alpha [f(\varepsilon_l - \varepsilon_{l'} - \mu_\alpha)|\langle l'|d_{i\sigma}|l\rangle|^2 - (1 - f(\varepsilon_{l'} - \varepsilon_l - \mu_\alpha))|\langle l|d_{i\sigma}|l'\rangle|^2]. \quad (19)$$

One can notice that the spin-dependent current stems from the spin-selection rule $\langle l|d_{i\sigma}|l'\rangle$, namely,

$$\langle l'|d_{1\uparrow}|l\rangle = \sum_{n_2^\sigma n_\mathrm{M}^\sigma} \beta^*_{0n_2^\sigma n_\mathrm{M}^\sigma} \beta_{\uparrow n_2^\sigma n_\mathrm{M}^\sigma} \langle 0 n_2^\sigma n_\mathrm{M}^\sigma|d_{1\uparrow}|\uparrow n_2^\sigma n_\mathrm{M}^\sigma\rangle,$$

$$\langle l'|d_{1\downarrow}|l\rangle = \sum_{n_2^\sigma n_\mathrm{M}^\sigma} \beta^*_{0n_2^\sigma n_\mathrm{M}^\sigma} \beta_{\downarrow n_2^\sigma n_\mathrm{M}^\sigma} \langle 0 n_2^\sigma n_\mathrm{M}^\sigma|d_{1\downarrow}|\downarrow n_2^\sigma n_\mathrm{M}^\sigma\rangle. \quad (20)$$

Here, $\beta_{n_1^\sigma n_2^\sigma n_\mathrm{M}^\sigma}$ is the expansion coefficient of $|l\rangle$ on the basis and $\beta_{\uparrow n_2^\sigma n_\mathrm{M}^\sigma} \neq \beta_{\downarrow n_2^\sigma n_\mathrm{M}^\sigma}$ due to spin splitting $\varepsilon_{2\sigma}$. As usual, the spin current is defined as $I_{\alpha\mathrm{s}} = I_{\alpha\uparrow} - I_{\alpha\downarrow}$ and the charge current is defined as $I_{\alpha\mathrm{c}} = I_{\alpha\uparrow} + I_{\alpha\downarrow}$.

In Fig. 5, we display the spin-dependent currents $I_{\mathrm{R}\uparrow}$ and $I_{\mathrm{R}\downarrow}$ as a function of ε_1. Obviously, at $\varepsilon_1 = \varepsilon_{2\downarrow} = 0.5$ meV, a large spin current I_{Rs} and a small charge current I_{Rc} appear due to the opposite signs for $I_{\mathrm{R}\uparrow}$ and $I_{\mathrm{R}\downarrow}$. If one chooses appropriate μ_R, as shown in Fig. 5(b), a pure spin current can be realized at certain μ_R, where $I_{\mathrm{Rc}} = 0$ and $I_{\mathrm{Rs}} \neq 0$ (see point A in Fig. 5(b)). Similarly, at $\varepsilon_1 = -\varepsilon_{2\uparrow} = 0.5$ meV, a pure spin current is also obtained but with a different direction (see point B in Fig. 5(b)). At the same time, one can notice that when a pure spin current is realized in the right lead, the spin filter effect (existence of the current of only one spin component and the other vanishing) is present in the left lead, which is indicated in the inset of Fig. 5(a).

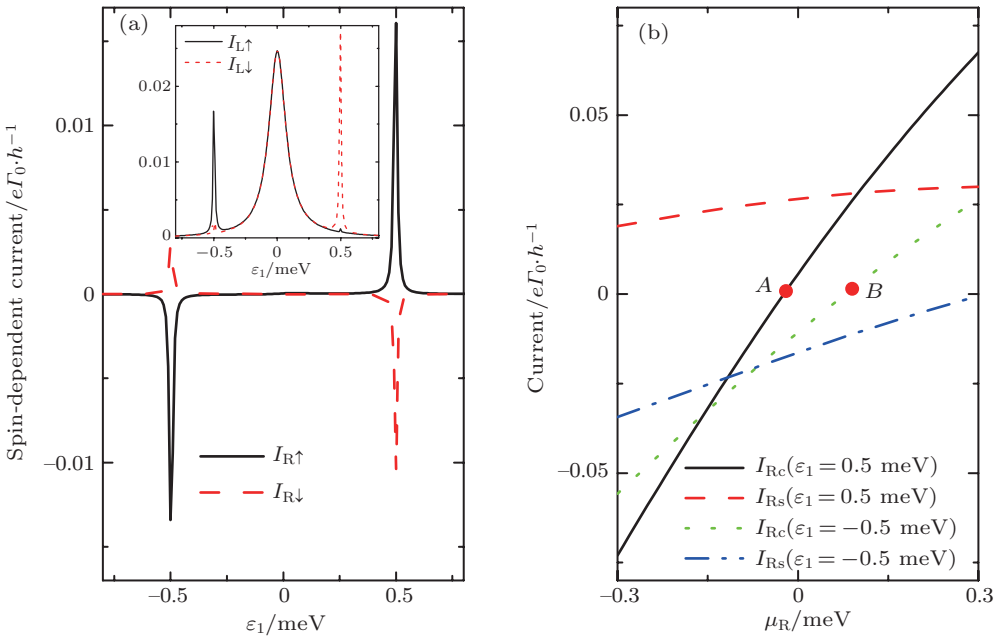


Fig. 5. (color online) (a) Spin-dependent currents $I_{\mathrm{R}\sigma}$ as a function of ε_1 with $\mu_\mathrm{R} = -0.1$ mV, and (b) spin currents I_{Rs} and charge currents I_{Rc} versus μ_R for $\varepsilon_1 = 0.5$ meV and -0.5 meV. Other parameters are $\mu_\mathrm{L} = 0.2$ mV, $t_0 = \Delta_0 = 0.03$ meV, $\varepsilon_2 = 0, \varepsilon_\mathrm{M} = 0, \Delta_\mathrm{B} = 1$ meV, $k_\mathrm{B}T_0 = 0.5$ meV, and $\Gamma_0 = 0.01$ meV expected for the specific indication.

4. Experimental feasibility

Epitaxially grown InSb quantum dots may be suitable materials to form the excitation of Majorana fermions, since InSb possesses a large electron g factor ($|g^*| \sim 30$–70) and a strong spin–orbit interaction (with energy $\Delta_\mathrm{SOI} \sim 0.3$ meV).[43] Therefore, for possible experimental demonstration, the system could be built by placing InSb quantum dots on an s-wave superconductor substrate (with superconducting gap $\Delta \sim 0.2$ meV) under an external applied magnetic field of a moderate strength (0.15 T). The diameter of the quantum dot is about 200 nm, while the coherent length of a superconductor is approximately 216 nm, electrons therefore can tunnel between neighboring dots either through normal tunneling with coupling strength $t_{1(2)}$ or CAR with pairing potential $\Delta_{1(2)}$ induced by the superconductor. Nevertheless, the two outmost dots are disconnected with each other because the distance between them is beyond the superconductor's coherent length.

Under these conditions, the model proposed in our paper can be realized. The energy level of the quantum dots, in reality, can be modulated by gate voltages, and the tunneling rates $\Gamma_{L(R)}$ and coupling strength $t_{L(R)}$ can also be controlled by utilizing the gate-voltage technique. As for the chemical potential $\mu_{L(R)}$, we can tune them independently when two power sources are applied, respectively, between lead L coupling to dot 1 (or lead R coupling to dot 2) and the superconductor.

5. Concluding remarks

We study the transport properties through a setup with three QDs hybridized with conventional s-wave superconductors. By tuning the dot levels, we present the realization of MFs and show that the MFs either locate on different dots separately, or distribute themselves among different dots with tunable possibilities, depending on the relative positions of the dot levels. As a consequence, the nonequilibrium electronic transports show rich physical mechanisms, including the LAR, CAR, and CRT. These mechanisms are modulated by the Majorana states and can be switched to each other by tuning the system parameters, which reveals the unique properties of Majorana fermions. In addition, spin-polarized transports are discussed. Interestingly, we find a pure spin current and a spin filter effect originating from the joint effect of CRT and CAR. We expect that our findings will be helpful for experimentally detecting MFs and designing spintronic devices.

References

[1] Sato M, Takahashi Y and Fujimoto S 2009 *Phys. Rev. Lett.* **103** 020401
[2] Alicea J 2010 *Phys. Rev. B* **81** 125318
[3] Lutchyn R M, Sau J D and Das Sarma S 2010 *Phys. Rev. Lett.* **105** 077001
[4] Oreg Y, Refael G and von Oppen F 2010 *Phys. Rev. Lett.* **105** 177002
[5] Sau J D, Lutchyn R M, Tewari S and Das Sarma S 2010 *Phys. Rev. Lett.* **104** 040502
[6] Fu L and Kane C L 2008 *Phys. Rev. Lett.* **100** 096407
[7] Nayak C, Simon S H, Stern A, Freedman M and Sarma S D 2008 *Rev. Mod. Phys.* **80** 1083
[8] Stern A 2010 *Nature* **464** 187
[9] Alicea J, Oreg Y, Refael G, von Oppen F and Fisher M P A 2011 *Nat. Phys.* **7** 412
[10] Liu D E and Baranger H U 2011 *Phys. Rev. B* **84** 201308(R)
[11] Deng M T, Yu C L, Huang G Y, Larsson M, Caroff P and Xu H Q 2012 *Nano Lett.* **12** 6414
[12] Qi X L and Zhang S C 2011 *Rev. Mod. Phys.* **83** 1057
[13] Fu L and Kane C L 2009 *Phys. Rev. B* **79** 161408(R)
[14] Liu Y, Ma Z, Zhao Y F, Meenakshi S and Wang J 2013 *Chin. Phys. B* **22** 067302
[15] He K, Ma X C, Chen X, Lü L, Wang Y Y and Xue Q K 2013 *Chin. Phys. B* **22** 067305
[16] Yuan J H, Cheng Z, Zhang J J, Zeng Q J and Zhang J P 2012 *Chin. Phys. B* **21** 047203
[17] Kitaev A Y 2001 *Phys. Usp.* **44** 131
[18] Sau J D and Das Sarma S 2012 *Nat. Commun.* **3** 964
[19] Fulga I C, Haim A, Akhmerov A R and Oreg Y 2013 *New J. Phys.* **15** 045020
[20] Leijnse M and Flensberg K 2012 *Phys. Rev. B* **86** 134528
[21] Bolech C J and Demler E 2007 *Phys. Rev. Lett.* **98** 237002
[22] Law K T, lee P A and Ng T K 2009 *Phys. Rev. Lett.* **103** 237001
[23] Nilsson J, Akhmerov A R and Beenakker C W J 2008 *Phys. Rev. Lett.* **101** 120403
[24] Strübi G, Belzig W, Choi M S and Bruder C 2011 *Phys. Rev. Lett.* **107** 136403
[25] Cao Y, Wang P, Xiong G, Gong M and Li X Q 2012 *Phys. Rev. B* **86** 115311
[26] Wang P, Cao Y, Gong M, Xiong G and Li X Q 2013 *Europhys. Lett.* **103** 57016
[27] Lü H F, Lu H Z and Shen S Q 2012 *Phys. Rev. B* **86** 075318
[28] Zocher B and Rosenow B 2013 *Phys. Rev. Lett.* **111** 036802
[29] Pötlt C, Emary C and Brandes T 2009 *Phys. Rev. B* **80** 115313
[30] Leijnse M and Flensberg K 2011 *Phys. Rev. B* **84** 140501
[31] Žitko R and Simon P 2011 *Phys. Rev. B* **84** 195310
[32] Lee M, Lim J S and López R 2013 *Phys. Rev. B* **87** 241402(R)
[33] Leijinse M and Flensberg K 2011 *Phys. Rev. Lett.* **107** 210502
[34] Shang E M, Pan Y M, Shao L B and Wang B G 2014 *Chin. Phys. B* **23** 057201
[35] Wright A R and Veldhorst M 2013 *Phys. Rev. Lett.* **111** 096801
[36] Emary C, Pötlt C and Brandes T 2009 *Phys. Rev. B* **80** 235321
[37] Lu H Z, Zhou B and Shen S Q 2009 *Phys. Rev. B* **79** 174419
[38] Cottet A, Belzig W and Bruder C 2004 *Phys. Rev. Lett.* **92** 206801
[39] Djuric I, Dong B and Cui H L 2005 *IEEE Trans. Nanotechnol.* **4** 71
[40] Wang R Q, Sheng L, Hu L B, Wang B G and Xing D Y 2011 *Phys. Rev. B* **84** 115304
[41] Pan H, Li Z S and Lü R 2013 *Chin. Phys. Lett.* **30** 087102
[42] Ying Y B and Jin G J 2010 *Appl. Phys. Lett.* **96** 093104
[43] Deng M T, Yu C L, Huang G Y, Larsson M, Caroff P and Xu H Q 2012 *Nano Lett.* **12** 6414